Stress-Induced Neural Plasticity Mediated by Glial GPCR REMO-1 Promotes *C. elegans* Adaptive Behavior

In Hae Lee[1], **Carl Procko**[1,2], **Yun Lu**[1], **Shai Shaham**[1,3,*]

[1]Laboratory of Developmental Genetics, The Rockefeller University, 1230 York Avenue, New York, NY 10065, USA

[2]Present address: The Salk Institute for Biological Studies, PBIO-C, 10010 N. Torrey Pines Road, La Jolla, CA 92037, USA

[3]Lead Contact

SUMMARY

Animal nervous systems remodel following stress. Although global stress-dependent changes are well documented, contributions of individual neuron remodeling events to animal behavior modification are challenging to study. In response to environmental insults, *C. elegans* become stress-resistant dauers. Dauer entry induces amphid sensory organ remodeling in which bilateral AMsh glial cells expand and fuse, allowing embedded AWC chemosensory neurons to extend sensory receptive endings. We show that amphid remodeling correlates with accelerated dauer exit upon exposure to favorable conditions and identify a G protein-coupled receptor, REMO-1, driving AMsh glia fusion, AWC neuron remodeling, and dauer exit. REMO-1 is expressed in and localizes to AMsh glia tips, is dispensable for other remodeling events, and promotes stress-induced expression of the remodeling receptor tyrosine kinase VER-1. Our results demonstrate how single-neuron structural changes affect animal behavior, identify key glial roles in stress-induced nervous system plasticity, and demonstrate that remodeling primes animals to respond to favorable conditions.

Graphical Abstract

AMsh glia (green)
AWC neuron (magenta)
Unfused glia → Late dauer exit
REMO-1
Fused glia → Early dauer exit
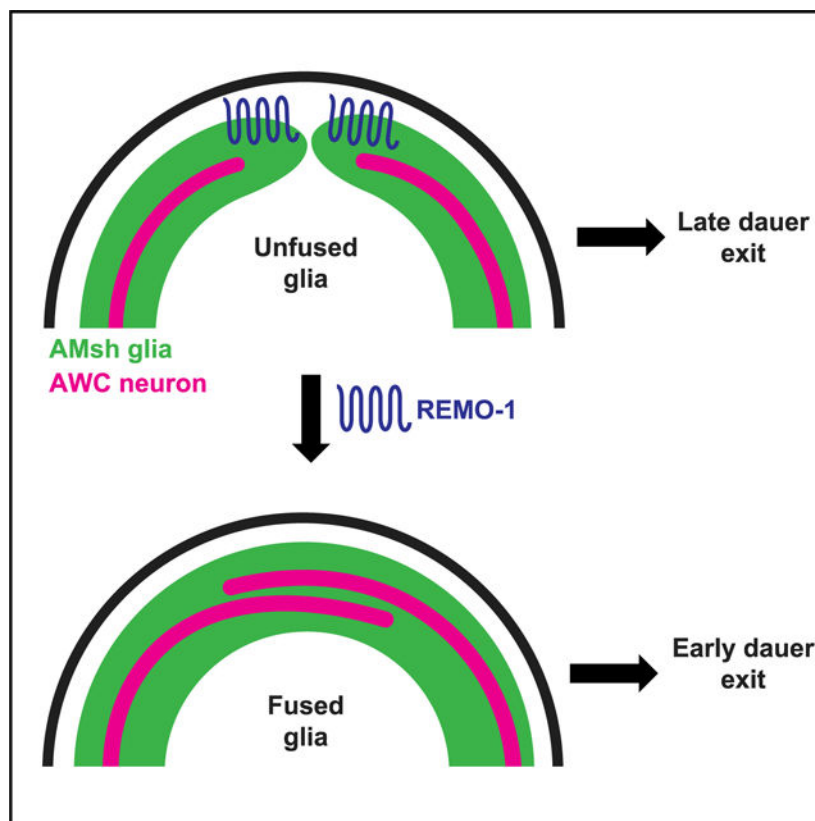
In Brief

Lee et al. provide molecular insight into how stress-induced sensory organ remodeling affects behavior in *C. elegans.* They identify a glial GPCR, REMO-1, that drives structural remodeling of sensory neurons and associated glia. This alteration of a single neuron-glia pair primes animals to respond efficiently to favorable environmental conditions.

INTRODUCTION

Nervous systems are robust in connectivity (Goodman and Shatz, 1993), allowing reproducibility in behavior, yet malleable in function, permitting adaptation to fluctuating environments (Albert and Riddle, 1983; Bourne and Harris, 2008; Cuschieri and Bannister, 1975; Engström, 1967; Flock et al., 1999; Golden and Riddle, 1984; Goodman and Shatz, 1993; Murray, 1993; Procko et al., 2011). Such plasticity can be accompanied by structural alterations. For example, in response to dehydration or lactation, astrocytes retract their synapse-associated processes in the paraventricular and supraoptic nuclei to alter synaptic activity (Chapman et al., 1986; Gregory et al., 1980; Hatton et al., 1984; Theodosis et al., 1986; Theodosis and Poulain, 1984, 1989). Similarly, environmental stimuli remodel sensory organs. For example, in the organ of Corti of the mammalian inner ear, glia-like Deiters' cells form a scaffold that supports outer hair cells (Rio et al., 2002). Upon exposure to high-intensity sound, Deiters' glia are displaced toward outer hair cells to reduce cochlear sensitivity, protecting against hearing loss (Flock et al., 1999).

Changes in animal behavior have been correlated with large-scale changes in glia and neuron ensembles, and plasticity mechanisms in individual neurons have been extensively explored (Citri and Malenka, 2008). However, linking changes at single synapses or at single sensory receptive endings to animal behavior, a major goal for understanding neural processing, is challenging in animals in which many neurons contribute to behavior.

The nematode *C. elegans* is an excellent model in which to study sensory organ remodeling and single-cell contributions to animal behavior. Upon exposure to stressful conditions, including high temperature, starvation, and crowding, animals enter an alternative developmental state called dauer (Cassada and Russell, 1975; Golden and Riddle, 1984). The sensory nervous system of dauer animals undergoes striking changes in morphology and gene expression. These changes have been studied primarily in the context of the amphid and inner labial sensilla (Albert and Riddle, 1983; Peckol et al., 2001; Schroeder et al., 2013). Amphids are the primary *C. elegans* sensory organs, detecting chemosensory, osmotic, mechanical, thermal, light, and other stimuli (Bargmann and Mori, 1997; Perkins et al., 1986; Troemel, 1999; Troemel et al., 1995). Each of the bilateral amphids consists of 12 sensory neurons and two glial cells, the AMsh and AMso glial cells, which wrap around sensory neuron receptive endings (NREs) (Ward et al., 1975). Under normal growth conditions, the NRE of each of the bilateral AWC amphid neurons, which houses receptors for volatile odorants (Troemel, 1999; Troemel et al., 1995), is individually ensheathed by processes of adjacent AMsh glial cells (Figures 1A and 1B). Upon dauer entry, AWC NREs expand along with their associated AMsh glia wrappings. In half of dauer animals, bilateral AMsh glia fuse, allowing AWC NREs to expand beyond the midline (Figure 1C) (Albert and Riddle, 1983; Golden and Riddle, 1984; Procko et al., 2011). Thus, AMsh glia delimit AWC NRE growth. Ablation studies demonstrate that AMsh glia remodel independently of AWC NREs (Procko et al., 2011). The functional consequences of AMsh glia and AWC neuron alterations in dauers are not known.

Previous studies from our lab identified several AMsh glia proteins implicated in remodeling. These include the cell fusion protein AFF-1; a VEGFR-related tyrosine kinase protein, VER-1; the Otd/Otx transcription factor TTX-1; and the zinc finger transcription factor ZTF-16 (Procko et al., 2011, 2012). *ver-1* expression in AMsh glia is induced by cultivation at high temperature (25°C) or by dauer entry and requires direct binding of TTX-1 to *ver-1* regulatory sequences (Procko et al., 2011).

Here we demonstrate that amphid sensory organ remodeling correlates with early dauer exit following exposure to a favorable environment. We identify a gene, *remo-1* (*remo*deling defective-*1*), encoding a putative 7-transmembrane G protein-coupled receptor (GPCR) that is required for dauer-induced AMsh glia and AWC neuron remodeling. REMO-1 protein is required for expression of VER-1 in AMsh glia, functions in and is expressed in AMsh glia, and localizes to the tip of amphid sensilla. Importantly, *remo-1* loss delays dauer exit behaviors. Our studies link shape changes in a single neuron-glia pair to animal behavior and demonstrate that glia-dependent nervous system remodeling following stress allows animals to efficiently detect restoration of a non-stressful environment.

RESULTS

Glial REMO-1 Regulates Stress-Induced VER-1/RTK Expression

To uncover genes required for AMsh glia and AWC neuron remodeling in dauer animals, we sought mutants that fail to induce *ver-1* promoter::GFP transgene expression in adults grown at 25°C (Procko et al., 2011). As *ver-1* is also upregulated in dauer animals and is implicated in AMsh glia remodeling (Procko et al., 2011), we reasoned that our screen might identify remodeling genes. Indeed, roles for *ttx-1* and *ztf-16* were discovered in this way (Procko et al., 2011, 2012). From this screen, we identified a mutant, with designated allele number *ns250*, that fails to turn on *ver-1*p::GFP in young adults cultivated at 25°C and in dauer larvae induced by starvation (Figures 2A and 2B). Genetic mapping and whole-genome sequencing showed that *ns250* is not an allele of previously identified remodeling genes. Rather, *ns250* mutants carry a lesion in the gene *F47D2.11*, which we have renamed *remo-1*. *remo-1* is a putative Srz-type GPCR (Figure 2C) and is conserved in other nematodes (Figure S1) (Robertson and Thomas, 2006). The functions of Srz GPCRs are not well understood. The *remo-1(ns250)* allele is predicted to cause a glutamic acid-to-lysine change at position 278 (E278K) in the C-terminal intracellular tail of the protein (Figure 2C). This residue is part of a threonine-glutamic acid-isoleucine (TEI) motif conserved in a subfamily of Srz GPCRs (Figure S1) and lies at the terminal membrane-cytosol interface (Figures 2C and S1), suggesting that its mutation could lead to REMO-1 function deficits.

To confirm that the E278K change is the causal mutation in *remo-1(ns250)* mutants, we recreated the same genomic lesion in otherwise wild-type animals carrying the *ver-1*p::GFP transgene using CRISPR. Two independent mutants, *remo-1(ns820, ns821)*, were isolated, and both fail to induce *ver-1*p::GFP expression in young adults cultivated at 25°C and in dauer larvae induced by starvation (Figures 2A and 2B). Furthermore, transgenes containing a genomic fosmid clone encompassing the *remo-1* locus, or a smaller genomic fragment, restore *ver-1*p::GFP expression to *remo-1(ns250)* mutants (Figure 2D). Finally, we found that expression of *remo-1* cDNA using an AMsh glia-specific promoter, derived from the *F16F9.3* gene, but not an amphid sensory neuron promoter, derived from the *dyf-7* gene, also restores *ver-1*p::GFP induction to *remo-1(ns250)* mutants (Figure 2D). Taken together, these results strongly support a role for *remo-1*, acting in AMsh glia, in the induction of *ver-1*p::GFP expression.

REMO-1 Functions in AMsh Glia to Regulate Dauer-Induced AMsh Glia Remodeling

We next sought to determine whether *remo-1* is required for AMsh glia remodeling in dauers. Remodeling is difficult to follow optically, as the structures in question are often separated by <20 nm. We therefore monitored remodeling functionally by assessing the frequency of fusion of the two AMsh glia, using a cytoplasmic mixing assay we previously developed (Figure 3A) (Procko et al., 2011). Briefly, *daf-7(e1372)* single or *daf-7(e1372)*; *remo-1(ns250)* double mutants, which, independently of crowding or starvation, become dauers at 25°C as a result of the *daf-7(e1372)* lesion, were engineered to carry an AMsh glia::GFP transgene from an unstable extrachromosomal array (*nsEx1391*). First-stage larvae (L1) of these strains that express GFP in only one of the bilateral AMsh glial cells were then isolated. These mosaic animals were cultivated at 25°C for 48 h to induce dauer

entry and scored for GFP redistribution to both cells, indicating fusion. Although 46% of *daf-7(e1372)* single mutants distribute GFP to both AMsh glia, consistent with our previous studies (Procko et al., 2011, 2012), no redistribution is seen in *daf-7(e1372)*; *remo-1(ns250)* double mutants (Figure 3B). Similarly, the CRISPR-generated strains, *remo-1(ns820)* and *remo-1(ns821)*, also show no GFP redistribution (Figure 3B). Consistent with these findings, *daf-7(e1372)* dauer animals that fail to redistribute GFP do not show fusion when examined by electron microscopy (EM) serial reconstructions (n = 3), while animals that distribute GFP do (n = 2; Figures 3C and 3D), and EM reconstructions of *daf-7(e1372)*; *remo-1(ns250)* double mutants reveal a lack of fusion (n = 2; Figure 3E). Importantly, as with *ver-1*p::GFP rescue, expressing REMO-1 in AMsh glia, but not in AWC and other amphid neurons, fully restores AMsh glia fusion to *remo-1(ns250)* mutants (Figure 3B). Thus, REMO-1 is required in AMsh glia for dauer-dependent AMsh glia remodeling and functions downstream of or in parallel to DAF-7/TGFβ.

REMO-1 Is Also Required for AWC Neuron Remodeling

As AMsh glia can affect sensory NRE morphology (Procko et al., 2011, 2012; Singhvi et al., 2016), we assessed whether REMO-1 regulates AWC remodeling using EM. In *ttx-1* mutant dauers, AWC neurons can expand within the limited space provided by each unfused AMsh glial cell by forming membrane loops to accommodate excess AWC growth (Figure 1D) (Procko et al., 2011). In these animals, AWC and AMsh glia remodeling are, therefore, uncoupled. In *ztf-16* mutants, AMsh glia and AWC NREs are not well developed in non-dauer animals and remain the same in dauer animals (Figure 1E) (Procko et al., 2012). In *remo-1(ns250, ns820, or ns821)* mutants, we found that AWC dendrites fill the unfused glial space but do not expand further to create the membrane loops observed in *ttx-1* mutants (n = 6; Figures 1D, 1F, and 3E), suggesting that *remo-1* is required for both AMsh fusion and AWC expansion.

To determine whether *remo-1* regulates other neuronal remodeling events, we examined IL2 sensory neurons, which exhibit dauer-dependent dendritic arborization (Schroeder et al., 2013). We found that 100% of *daf-7(e1372)* animals and 98% of *daf-7(e1372)*; *remo-1(ns250)* double mutants exhibit remodeling (Figures S2C–S2E). Thus, although *remo-1* controls dauer-induced AMsh glia and AWC remodeling, it does not control all remodeling events.

REMO-1 Is Expressed in AMsh Glia and Localizes to the Glial Tip

The *ver-1*p::GFP and AMsh glia fusion rescue studies suggest that REMO-1 is expressed in AMsh glia. To confirm this, we generated wild-type animals carrying a bicistronic transgene consisting of the *remo-1* genomic locus, including its 5′ intergenic region, and DNA encoding mKate2 fluorescent protein tagged with two nuclear localization signals, separated by a *trans*-splicing site (Figure 4A). We found that mKate2 expression is detected in AMsh glia of all larval stages, as confirmed by co-expression with a pan-glial *mir-228*p::myristoylGFP transgene (Figure 4B). We also detected rare expression in ASI and ASJ neurons (Figure S2), confirmed by DiO staining, but never in AWC neurons. Although ASI and ASJ control whole-animal dauer entry and exit (Bargmann and Horvitz, 1991; Cornils et al., 2011), *remo-1* mutants can form dauers at normal rates, and *remo-1* AMsh and

AWC remodeling defects are not rescued by expression of *remo-1* in these neurons (Figure 3B). The cell-autonomous functions of REMO-1, together with lack of REMO-1 expression in AWC neurons, suggest that AWC remodeling defects most likely follow from AMsh glia deficits.

To examine REMO-1 subcellular localization, we used CRISPR to knock in a transgene encoding Venus fluorescent protein sequences upstream of the *remo-1* stop codon (Figure 4A) (Arribere et al., 2014). Transgenic animals show consistent Venus expression in two adjacent regions at the tip of the nose in both dauer and non-dauer larvae (Figure 4C), consistent with localization at the site of AMsh glia and AWC remodeling events.

REMO-1 Differentially Regulates *ver-1* Transcription and Amphid Remodeling

To understand how REMO-1 functions with respect to previously identified remodeling genes, we examined expression of *ttx-1* and *ztf-16* and localization of AFF-1 in wild-type and *remo-1(ns250)* mutants. Using *ttx-1* and *ztf-1* transcriptional reporters, we measured the mean fluorescent intensity of GFP expression in the AMsh cell body in wild-type (n = 21 and n = 11, respectively) and *remo-1(ns250)* mutant (n = 21 and n = 12, respectively) backgrounds and found that *ttx-1* and *ztf-16* expression levels are unaffected by the *remo-1* mutation. We also quantified *ttx-1* and *ztf-16* expression frequencies and found no difference in the fraction of animals expressing *ttx-1* in AMsh glia in either wild-type (100% [n = 75]) or *remo-1(ns250)* mutant backgrounds (100% [n = 75]). Similarly, *ztf-16* expression frequency was unchanged in wild-type (100% [n = 50]) or *remo-1(ns250)* mutants (100% [n = 50]).

Likewise, AMsh glia-expressed AFF-1::GFP fusion protein localizes to the nose tip in wild-type animals (100% [n = 50]) and in *remo-1(ns250)* mutants (100% [n = 48]). Thus, *remo-1(n250)* affects *ver-1*p::GFP expression but not expression or localization of other genes driving remodeling.

Curiously, we found that *remo-1(ns843, ns844, and ns845)* predicted loss-of-function deletion alleles, as well as *remo-1(ns841 and ns842)* premature stop-codon insertion alleles we generated, do not perturb *ver-1* expression at 25°C or in dauer larvae but still block glia remodeling (Figures S3A–S3E). These observations suggest that the effect on *ver-1* expression is allele specific and demonstrate that *ver-1* expression can be uncoupled from dauer remodeling. This is consistent with our previous findings that mutations in *ver-1* do not fully block remodeling (Procko et al., 2011). Thus, REMO-1 likely acts upstream of additional remodeling pathways. AWC neurons also fail to remodel in these loss-of-function mutants (n = 4; Figure S3E), further suggesting that *remo-1*-dependent AMsh glia remodeling likely influences AWC remodeling.

REMO-1-Dependent Remodeling Facilitates Dauer Exit

The purpose of amphid remodeling in dauer animals has been debated. Previous studies demonstrated that amphid sensory neuron odorant receptor repertoire is altered in dauers (Peckol et al., 2001). This raises the possibility that dauers adjust sensory tuning to detect favorable environments, which would promote dauer exit behavior. We sought, therefore, to examine whether remodeling-defective animals exhibit dauer exit defects. In dauer animals,

pharyngeal pumping, used to suck in bacteria, ceases (Cassada and Russell, 1975; Chow et al., 2006), and pumping resumption is the first sign of dauer exit (Albert and Riddle, 1983). To assess dauer recovery, we therefore exposed animals to GFP-expressing bacteria, which promote dauer exit, and monitored pharyngeal GFP accumulation (Figures 4D and 4E). Accumulation coincides with the onset of pharyngeal pumping, as correlated by direct observation (Figure S4A) (Chou et al., 2015; Proudfoot et al., 1993), and can be used to quickly examine many animals at a time. We found that 50% of wild-type animals exit the dauer stage at 2.9 ± 0.3 h following bacterial food introduction, while *ttx-1* mutants, in which dauer-dependent AMsh glia remodeling is defective, exit dauer significantly later, with half of animals accumulating pharyngeal GFP at 4.0 ± 0.1 h (Figure 4F). Animals in which AWC neurons are ablated (Beverly et al., 2011), but in which AMsh glia fusion still occurs (Figure S4B), are even more severely delayed, with 50% recovering at 4.7 ± 0.1 h (Figure 4F). This is consistent with the observation that AWC neurons in *ttx-1* mutants still expand, albeit in a disorganized fashion (Procko et al., 2011). These results suggest that remodeling of AWC neurons may drive timely dauer exit behavior. However, *ttx-1* mutants also perturb neuronal temperature sensing, and AWC neuron ablations do not distinguish whether it is the presence or the specific remodeling of AWC neurons that is important. Therefore, we reasoned that *remo-1* mutants, which fail to remodel both AMsh glia and AWC neurons, and which do not exhibit other defects, are better suited for testing the effects of remodeling on dauer exit.

We found that following food exposure, 50% of *remo-1(ns250)* animals exit dauer at 4.6 ± 0.6 h, a similar delay to that observed in AWC-ablated animals (Figure 4F), supporting the idea that dauer remodeling is indeed required for efficient dauer exit. Importantly, restoring wild-type REMO-1 to AMsh glia of *remo-1(ns250)* animals not only restores AMsh glia fusion, and presumably AWC remodeling, but fully rescues dauer exit delay (Figure 4F). Expression of REMO-1 in amphid neurons does not (Figure 4F). Taken together, the correlation of remodeling dynamics and dauer exit are consistent with the view that these two processes are causally linked.

To determine whether glia remodeling affects dauer exit efficiency, we examined wild-type animals that exited dauer early (2 h) or late (4 h) following exposure to GFP-tagged OP50 bacteria. We then examined AMsh glia fusion in these animals using EM. In all animals that exited dauer early, left and right AMsh glial cells fused on both dorsal and ventral sides (n = 4). However, glial fusion was more variable in animals that exited dauer late. Here, we found one animal in which AMsh glia failed to fuse on both dorsal and ventral sides, one animal in which glial fusion occurred only on one side, and one animal with glial fusion on both sides. Thus, glial remodeling may facilitate efficient dauer exit upon exposure to favorable conditions.

DISCUSSION

The studies presented here provide insight into how sensory neurons and their associated glia remodel in response to a changing environment and demonstrate direct behavioral consequences of such plasticity. Correlating activities of single neurons, single synapses, or single sensory endings, with animal behavior is impossible in most model systems, as these

responses require activities of large neuronal ensembles. We show here that *C. elegans* provides a unique setting that allows direct interrogation of this black box regime, in which single-neuron, neuron-glia pair, or sensory structure perturbations lead to direct behavioral output.

Our data are consistent with a model in which REMO-1 acts in AMsh glia following detection of dauer entry cues to facilitate AMsh glia remodeling. This drives expansion of AWC neuron NREs, which, in turn, appears to promote efficient dauer exit following re-introduction of *C. elegans* to a favorable environment. REMO-1 functions in parallel to or downstream of DAF-7/TGFβ signaling and may therefore directly sense environmental cues promoting dauer entry. However, it may also respond to detection of such cues by sensory neurons, respond indirectly to downstream signaling induced by neuropeptides or insulin-like peptides important for dauer entry, become active in response to internal ligands, or exhibit constitutive activity, transducing signals only when downstream signaling machinery becomes available. Identification of REMO-1 ligands may help distinguish among these possibilities. Furthermore, our results suggest that REMO-1 likely has yet to be discovered targets, which may function in both AMsh glia and AWC neurons.

REMO-1 is a member of a small family of predicted *C. elegans* GPCRs with a unique C-terminal sequence. This raises the possibility that these other GPCRs might also participate in remodeling events. Interrogating the consequences of their loss may reveal such roles.

Finally, how REMO-1-mediated expansion of AWC neurons leads to accelerated dauer exit is a fascinating area for future investigation. This study, as well as our previous studies, reveals that AMsh glia fusion occurs in only 50% of wild-type dauer animals. Why this remodeling is not fully penetrant remains unclear. However, it is possible that it represents a way for animals to hedge their bets about the quality of a dauer exit signal. If dauers that remodel exit more quickly, and the environmental stimulus triggering exit is only transient, these animals would not go on to reproduce. However, un-remodeled dauer animals would not initiate dauer exit and would survive until a bona fide favorable environment is detected. In such a model, the increased surface area of AWC neurons could enhance their sensitivity to favorable environmental stimuli, perhaps by increasing the number of available receptors. Enhanced sensitivity could be used to detect volatiles from further away, or to compensate for the thicker cuticle of dauer animals, which may reduce odorant engagement with receptors. Our studies show that exposure to a dauer-exit stimulus for 4 h is sufficient to induce exit of both remodeled and un-remodeled animals. Thus, if remodeling is a mechanism for testing stimulus stability, persistence of the stimulus for 4 h must be a good predictive measure of longer-term stimulus stability in natural contexts.

STAR★METHODS

RESOURCE AVAILABILITY

Lead Contact—Further information and requests for resources and reagents should be directed to and will be fulfilled by the Lead Contact, Shai Shaham (shaham@rockefeller.edu).

Materials Availability—All unique/stable reagents generated in this study are available from the Lead Contact without restriction.

Data and Code Availability—This study did not generate any unique datasets or code.

EXPERIMENTAL MODEL AND SUBJECT DETAILS

C. elegans—*C. elegans* were cultivated using standard methods (Brenner, 1974). All animals were cultivated at 15°C or 25°C, unless otherwise noted. Bristol N2 strain was used as wild-type. Mutants recovered by Ethyl methanesulfonate (EMS) mutagenesis were outcrossed at least three times before use. Most strains had the *nsIs22* (*ver-1*p::GFP) IV reporter transgene. Co-injection markers used were *unc-122*p::GFP, *unc-122*p::RFP, or *unc-122*p::DsRed expressed in coelomocytes, or plasmids as otherwise noted. Integrated transgenic strains were generated with UV/trioxalen treatment (Mello et al., 1991) (Sigma, T6137). AWC neurons were ablated via cell-specific expression of caspases under *ceh-36* promoter sequences (Beverly et al., 2011). Some strains listed below were sourced from the CGC, funded by NIH Office of Research Infrastructure Programs (P40 OD010440).

Alleles used in this work are:

LGIII: *daf-7(e1372), unc-119(ed3)*

LGV: *ttx-1(p767), remo-1(ns250, ns820, ns821, ns841, ns842, ns843, ns844, ns845, ns846*[Venus])

LGX: *ztf-16(ns171)*

METHOD DETAILS

Forward Genetic Screen—Fourth-stage larvae carrying *nsIs22* in the N2 strain background were mutagenized with ethylmethanesulfonate (EMS) for 4 hours. Individual P0s were picked to separate 9cm NGM agar plates with seeded OP50. F2 animals were screened under a fluorescent dissecting scope (Leica) for mutants that failed to express *ver-1*p::GFP in the AMsh glia (Procko et al., 2011, 2012).

Gene Identification—A combination of Hawaiian Snip-SNP mapping (Wicks et al., 2001), and whole genome sequencing (Zuryn et al., 2010) using galign (Shaham, 2009) to align reads, was used to identify *remo-1(ns250)*. The *remo-1* mutation was confirmed by fosmid rescue (WRM0638cF08); *remo-1* genomic transgene rescue; and re-introduction of E278K CRISPR alleles.

Germline Transformation—Germline transformation was carried out as previously described (Mello and Fire, 1995). Plasmid mixes containing the plasmid of interest, co-injection markers, and pBluescript were injected into one or both gonads of young adult hermaphrodites (Mello and Fire, 1995). pBluescript was used to adjust the DNA concentration of injection mixes as necessary. Injected animals were singled onto NGM plates and allowed to grow for two generations. Transformed animals were picked onto single plates based on co-injection marker expression, and screened for stable inheritance of the extrachromosomal array. Only lines from different P_0 hermaphrodites were considered

independent. Isolated strains were staged based on morphology under a dissecting microscope and were screened for *ver-1*p::GFP expression, amphid remodeling, IL2 remodeling and/or dauer recovery.

Plasmid Construction—Plasmids were constructed using Gibson cloning into the applicable backbone plasmid (Gibson et al., 2009). *remo-1* cDNA was constructed by cloning each exon from the fosmid WRM0638cF08 and fusing in sequential order using Gibson cloning. *remo-1* promoter region includes the entire *remo-1* genomic locus, including its 5′ intergenic region. CRISPR-related vectors were generated using a site-directed mutagenesis protocol on plasmid pDD162 (Dickinson et al., 2013; Liu and Naismith, 2008).

Cytoplasmic Mixing Assay—AMsh glia fusion was observed using a fluorescence redistribution assay described in detail in Procko et al. (2011, 2012). First-stage mosaic larvae carrying the *nsEx1391* array in one of the two AMsh glia were picked onto fresh seeded plates. Mosaic animals were cultivated for at least 48 hours at 25°C to induce dauer entry due facilitated by *daf-7(e1372)* temperature-sensitive allele. Animals were only scored if they were dauer larvae by morphology at the end of the assay period. Mosaic animals were scored for redistribution of GFP to both cells, indicating fusion.

Dauer Selection—To induce dauer formation by starvation, embryos were collected by hypochlorite treatment and washed extensively in M9. Approximately 200 embryos were placed onto an NGM plate containing a small lawn of OP50 (~10 μL of saturated OP50, 24 hr before use). Embryos were allowed to hatch and develop at 15°C or 25°C into dauer larva. Failure to include OP50 on the plate resulted in animals that arrested as starved L1 stage larvae. Dauer animals were selected by treatment with 1% SDS in M9 solution for 15 min. Alternatively, young animals carrying the *daf-7(e1372)* mutation were induced to form dauers by incubation at 25°C.

Dauer Recovery Assay

Pharyngeal Pumping Assay: Dauer animals induced by starvation were individually selected onto a plate with a thick lawn of OP50 and incubated at 15°C. Dauers were examined every 30–60 min for consistent grinder movement, indicative of pharyngeal pumping, under the dissecting scope.

Uptake of GFP-Expressing Bacteria—OP50-GFP bacteria (CGC) were cultivated in LB media. 24 hr before the assay, approximately 40 μL of bacteria were plated evenly on the NGM plates and dried overnight in the dark at 15°C. Dauer animals induced by starvation were singled out on the seeded plate and cultivated at 15°C in the dark. Every 30–60 min, dauer animals were screened for GFP accumulation in the pharynx under the dissecting scope.

Dye Filling Assay—DiO (3,3′-dioctadecyloxacarbocyanine) (Sigma) stock solution was made at 5 mg/ml in N,N-dimethylformamide. Animals were stained with DiO (stock

solution diluted 1:10000 in M9 buffer) for 30–60 min, followed by three M9 washes to remove excess dye.

Generation of *remo-1* Alleles and Reporter Using CRISPR-Cas9 Genome Editing—Alleles of *remo-1* were generated using the co-CRISPR-based genome editing method as previously described (Arribere et al., 2014). pDD162 was used as a vector backbone and the following sgRNA sequences were added for each individual CRISPR attempt (E278K: 5′ TCCAGTGGTTGTCATGTGGA 3′; deletion and premature stop alleles: #1 (5′ GCGTTTGTTCAAGCAACATG 3′) and #2 (5′ AATTCTGAGTGTTTTGGTGA 3′)) to generate *remo-1* targeting vectors. A *dpy-10* sgRNA-pDD162-based vector was also generated (5′ GCTACCATAGGCACCACGAG 3′). Single-stranded repair oligos were ordered from Sigma (E279K: 5′ TATTTGTGAGTATCGATTTCTTCCTTGTTCCAGTGGTTGTCATGTGGACGaAAATCA AAGCGAACCCGGGTGTTATTCAGATTTTTGCAATTAACAACAAA 3′; *dpy-10*(*cn64*): 5′ CACTTGAACTTCAATACGGCAAGATGAGAATGACTGGAAACCGTACCGCATGCGG TGCCTATGGTAGCGGAGCTTCACATGGCTTCAGACCAACAGCCTAT 3′) (Arribere et al., 2014). N2 animals were injected with the following mix: 50 ng/μl *dpy-10* sgRNA, 50 ng/ μl *remo-1*[E278K] targeting vector (or a mix of 25 ng/μl *remo-1*[deletion/premature stop] targeting vector #1 and 25 ng/μl *remo-1*[deletion/premature stop] targeting vector #2), 20 ng/ μl *dpy-10*(*cn64*) repair oligo, and 20 ng/μl *remo-1* [E278K] repair oligo (when appropriate) in 1x injection buffer (20 mM potassium phosphate, 3 mM potassium citrate, 2% PEG, pH 7.5). F1 animals with Dpy or Rol phenotypes were picked to individual plates, indicating a CRISPR-based editing event had occurred. F1 animals were allowed to lay eggs, and then genotyped for successful co-conversion of the *remo-1* locus using PCR and restriction enzyme screening or Cel1 digestion of heteroduplex DNA (Ward, 2015). Non-Rol, non-Dpy F2 animals were then singled and homozygosed for the *remo-1* mutation or deletion.

The Venus reporter was generating by using Cas9-triggered homologous recombination (Dickinson et al., 2013). Venus sgRNA sequence (5′ ACGGAAATCAAAGCGAACCC 3′) and homologous Venus repair template (5′ 1.49kb homolog arm of the 3′ end of *remo-1* coding sequence)-*loxP*-reversed *unc-119*(+) cassette-*loxP*-Venus transgene-1.5kb *remo-1* downstream homology arm 3′) were used to insert the Venus reporter transgene at the 3′ end of *remo-1* sequence. DP38(*unc-119*(*ed3*)) animals were injected with the following mix: 10 ng/μl pGH8 (*rab-3*p::mCherry, Addgene #19359), 5 ng/μl pCFJ104 (*myo-3*p::mCherry, Addgene #19328), 2.5 ng/μl pCFJ90 (*myo-2*p::mCherry, Addgene #19327), 50 ng/μl REMO-1::VENUS targeting vector, 10 ng/μl Venus repair oligo in 1x injection buffer (20 mM potassium phosphate, 3 mM potassium citrate, 2% PEG, pH 7.5). Three injected worms per plate were left to starve for 2 weeks at 25°C. Non-red animals were picked individually and allowed to lay eggs, and then genotyped for successful insertion. The *loxP*-*unc-119*(+)-*loxP* cassette was subsequently removed by injecting the following mix: 50 ng/μl pDD104 (*eft-3*::*Cre*::*tbb-2* 3′UTR; Addgene #47551), 2.5 ng/μl pCFJ90 (*myo-2*p::mCherry, Addgene #19327), 47.5 ng/μl pBluescript in EB buffer. The animals in which the *unc-119*(+) gene was excised were isolated and confirmed by DNA sequence analysis. The

unc-119(*ed3*) mutation was then crossed out. Removing the *unc-119*(+) cassette did not change Venus expression pattern.

Microscopy and Image Processing—*ver-1*p::GFP (*nsIs22*) expression was assayed using a fluorescence dissecting microscope (Leica). Young adult hermaphrodites or dauer animals were scored. Compound microscope images were taken on an Axioplan II microscope using an AxioCam CCD camera (Zeiss) and analyzed using the Axiovision software (Zeiss). Some images were collected on a DeltaVision Core imaging system (Applied Precision) with a PlanApo 603/1.42 na or UPlanSApo 60x/1.3 oil-immersion objective and a Photometrics CoolSnap HQ camera (Roper Scientific). Images were deconvolved using softWoRx program (GE Healthcare).

ttx-1 and *ztf-16* expression levels were assayed using transcriptional reporter transgenes *nsEx1942* and *nsEx3001*, respectively. Using ImageJ, we hand-traced the AMsh cell body at the focal point section and measured the mean fluorescent intensity in wild-type and *remo-1(ns250)* mutant backgrounds. For AFF-1, we examined the *nsEx2727* transgene, an AMsh glia-expressed AFF-1::GFP fusion protein, and examined protein localization at the tip of the nose.

Electron Microscopy—Dauer animals for electron microscopy were grown at 25°C and selected for AMsh glial fusion or no fusion based on GFP fluorescence (see cytoplasmic mixing assay for more details). Animals were prepped and sectioned using standard methods (Lundquist et al., 2001). Imaging was acquired with a FEI Tecnai G2 Spirit BioTwin transmission electron microscope equipped with a 4K digital camera. The image acquisition, processing, and analysis was performed by using the SerialEM and IMOD software (Schorb et al., 2019).

QUANTIFICATION AND STATISTICAL ANALYSIS

Statistical analysis was performed using GraphPad Prism. Sample sizes and statistical parameters are reported in the main text, figures, and figure legends. When comparing a transgenic line to the parental strain, a minimum of three independent lines were scored. Data is judged to be statistically significant when $p < 0.05$ by unpaired t test or one-way ANOVA followed by Tukey's test where appropriate. The rates of the onset of GFP-tagged bacteria accumulation in the pharynx were plotted as survival from dauer and were compared by log-rank test using GraphPad Prism 8.

Protein Structure Prediction—Prediction of protein structure generated using Protter software (Omasits et al., 2014)

Multiple Sequence Alignment—A subfamily of Srz predicted GPCR amino acid sequences were aligned using Jalview v.2.11 (Waterhouse et al., 2009)

Supplementary Material

Refer to Web version on PubMed Central for supplementary material.

ACKNOWLEDGMENTS

REFERENCES

Albert PS, and Riddle DL (1983). Developmental alterations in sensory neuroanatomy of the Caenorhabditis elegans dauer larva. J. Comp. Neurol 219, 461–481. [PubMed: 6643716]

Arribere JA, Bell RT, Fu BXH, Artiles KL, Hartman PS, and Fire AZ (2014). Efficient marker-free recovery of custom genetic modifications with CRISPR/Cas9 in Caenorhabditis elegans. Genetics 198, 837–846. [PubMed: 25161212]

Bargmann CI, and Horvitz HR (1991). Control of larval development by chemosensory neurons in Caenorhabditis elegans. Science 251, 1243–1246. [PubMed: 2006412]

Bargmann CI, and Mori I (1997). Chemotaxis and Thermotaxis (Cold Spring Harbor, NY: Cold Spring Harbor Laboratory Press).

Beverly M, Anbil S, and Sengupta P (2011). Degeneracy and neuromodulation among thermosensory neurons contribute to robust thermosensory behaviors in Caenorhabditis elegans. J. Neurosci 31, 11718–11727. [PubMed: 21832201]

Bourne JN, and Harris KM (2008). Balancing structure and function at hippocampal dendritic spines. Annu. Rev. Neurosci 31, 47–67. [PubMed: 18284372]

Brenner S (1974). The genetics of Caenorhabditis elegans. Genetics 77, 71–94. [PubMed: 4366476]

Cassada RC, and Russell RL (1975). The dauerlarva, a post-embryonic developmental variant of the nematode Caenorhabditis elegans. Dev. Biol 46, 326–342. [PubMed: 1183723]

Chapman DB, Theodosis DT, Montagnese C, Poulain DA, and Morris JF (1986). Osmotic stimulation causes structural plasticity of neurone-glia relationships of the oxytocin but not vasopressin secreting neurones in the hypothalamic supraoptic nucleus. Neuroscience 17, 679–686. [PubMed: 2422593]

Chou HT, Vazquez RG, Wang K, Campbell R, Milledge GZ, Walthall WW, and Johnson CM (2015). HES-mediated repression of Pten in Caenorhabditis elegans. G3 (Bethesda) 5, 2619–2628. [PubMed: 26438299]

Chow DK, Glenn CF, Johnston JL, Goldberg IG, and Wolkow CA (2006). Sarcopenia in the Caenorhabditis elegans pharynx correlates with muscle contraction rate over lifespan. Exp. Gerontol 41, 252–260. [PubMed: 16446070]

Citri A, and Malenka RC (2008). Synaptic plasticity: multiple forms, functions, and mechanisms. Neuropsychopharmacology 33, 18–41. [PubMed: 17728696]

Cornils A, Gloeck M, Chen Z, Zhang Y, and Alcedo J (2011). Specific insulin-like peptides encode sensory information to regulate distinct developmental processes. Development 138, 1183–1193. [PubMed: 21343369]

Cuschieri A, and Bannister LH (1975). The development of the olfactory mucosa in the mouse: electron microscopy. J. Anat 119, 471–498. [PubMed: 1141050]

Dickinson DJ, Ward JD, Reiner DJ, and Goldstein B (2013). Engineering the Caenorhabditis elegans genome using Cas9-triggered homologous recombination. Nat. Methods 10, 1028–1034. [PubMed: 23995389]

Engström H (1967). The ultrastructure of the sensory cells of the cochlea. J. Laryngol. Otol 81, 687–715. [PubMed: 4961642]

Flock A, Flock B, Fridberger A, Scarfone E, and Ulfendahl M (1999). Supporting cells contribute to control of hearing sensitivity. J. Neurosci 19, 4498–4507. [PubMed: 10341250]

Gibson DG, Young L, Chuang R-Y, Venter JC, Hutchison CA 3rd, and Smith HO (2009). Enzymatic assembly of DNA molecules up to several hundred kilobases. Nat. Methods 6, 343–345. [PubMed: 19363495]

Golden JW, and Riddle DL (1984). The Caenorhabditis elegans dauer larva: developmental effects of pheromone, food, and temperature. Dev. Biol 102, 368–378. [PubMed: 6706004]

Goodman CS, and Shatz CJ (1993). Developmental mechanisms that generate precise patterns of neuronal connectivity. Cell 72 (Suppl), 77–98. [PubMed: 8428376]

Gregory WA, Tweedle CD, and Hatton GI (1980). Ultrastructure of neurons in the paraventricular nucleus of normal, dehydrated and rehydrated rats. Brain Res. Bull 5, 301–306. [PubMed: 7397574]

Hatton GI, Perlmutter LS, Salm AK, and Tweedle CD (1984). Dynamic neuronal-glial interactions in hypothalamus and pituitary: implications for control of hormone synthesis and release. Peptides 5 (Suppl 1), 121–138. [PubMed: 6384946]

Liu H, and Naismith JH (2008). An efficient one-step site-directed deletion, insertion, single and multiple-site plasmid mutagenesis protocol. BMC Biotechnol. 8, 91. [PubMed: 19055817]

Lundquist EA, Reddien PW, Hartwieg E, Horvitz HR, and Bargmann CI (2001). Three C. elegans Rac proteins and several alternative Rac regulators control axon guidance, cell migration and apoptotic cell phagocytosis. Development 128, 4475–4488. [PubMed: 11714673]

Mello C, and Fire A (1995). DNA transformation. Methods Cell Biol. 48, 451–482. [PubMed: 8531738]

Mello CC, Kramer JM, Stinchcomb D, and Ambros V (1991). Efficient gene transfer in C.elegans: extrachromosomal maintenance and integration of transforming sequences. EMBO J. 10, 3959–3970. [PubMed: 1935914]

Murray RG (1993). Cellular relations in mouse circumvallate taste buds. Microsc. Res. Tech 26, 209–224. [PubMed: 8241560]

Omasits U, Ahrens CH, Müller S, and Wollscheid B (2014). Protter: interactive protein feature visualization and integration with experimental proteomic data. Bioinformatics 30, 884–886. [PubMed: 24162465]

Peckol EL, Troemel ER, and Bargmann CI (2001). Sensory experience and sensory activity regulate chemosensory receptor gene expression in Caenorhabditis elegans. Proc. Natl. Acad. Sci. U S A 98, 11032–11038. [PubMed: 11572964]

Perkins LA, Hedgecock EM, Thomson JN, and Culotti JG (1986). Mutant sensory cilia in the nematode Caenorhabditis elegans. Dev. Biol 117, 456–487. [PubMed: 2428682]

Procko C, Lu Y, and Shaham S (2011). Glia delimit shape changes of sensory neuron receptive endings in C. elegans. Development 138, 1371–1381. [PubMed: 21350017]

Procko C, Lu Y, and Shaham S (2012). Sensory organ remodeling in Caenorhabditis elegans requires the zinc-finger protein ZTF-16. Genetics 190, 1405–1415. [PubMed: 22298710]

Proudfoot L, Kusel JR, Smith HV, Harnett W, Worms MJ, and Kennedy MW (1993). Rapid changes in the surface of parasitic nematodes during transition from pre- to post-parasitic forms. Parasitology 107, 107–117. [PubMed: 8355993]

Rio C, Dikkes P, Liberman MC, and Corfas G (2002). Glial fibrillary acidic protein expression and promoter activity in the inner ear of developing and adult mice. J. Comp. Neurol 442, 156–162. [PubMed: 11754168]

Robertson HM, and Thomas JH (2006). The putative chemoreceptor families of C. elegans. In WormBook: The Online Review of C. Elegans Biology http://www.wormbook.org/chapters/www_putativechemoreceptorfam/putativechemoreceptorfam.pdf.

Schneider CA, Rasband WS, and Eliceiri KW (2012). NIH Image to ImageJ: 25 years of image analysis. Nat. Methods 9, 671–675. [PubMed: 22930834]

Schorb M, Haberbosch I, Hagen WJH, Schwab Y, and Mastronarde DN (2019). Software tools for automated transmission electron microscopy. Nat. Methods 16, 471–477. [PubMed: 31086343]

Schroeder NE, Androwski RJ, Rashid A, Lee H, Lee J, and Barr MM (2013). Dauer-specific dendrite arborization in C. elegans is regulated by KPC-1/Furin. Curr. Biol 23, 1527–1535. [PubMed: 23932402]

Shaham S (2009). galign: a tool for rapid genome polymorphism discovery. PLoS ONE 4, e7188. [PubMed: 19779626]

Singhvi A, Liu B, Friedman CJ, Fong J, Lu Y, Huang X-Y, and Shaham S (2016). A glial K/Cl transporter controls neuronal receptive ending shape by chloride inhibition of an rGC. Cell 165, 936–948. [PubMed: 27062922]

Theodosis DT, and Poulain DA (1984). Evidence that oxytocin-secreting neurones are involved in the ultrastructural reorganisation of the rat supraoptic nucleus apparent at lactation. Cell Tissue Res. 235, 217–219. [PubMed: 6365328]

Theodosis DT, and Poulain DA (1989). Neuronal-glial and synaptic plasticity in the adult rat paraventricular nucleus. Brain Res. 484, 361–366. [PubMed: 2713693]

Theodosis DT, Chapman DB, Montagnese C, Poulain DA, and Morris JF (1986). Structural plasticity in the hypothalamic supraoptic nucleus at lactation affects oxytocin-, but not vasopressin-secreting neurones. Neuroscience 17, 661–678. [PubMed: 2422592]

Troemel ER (1999). Chemosensory signaling in C. elegans. BioEssays 21, 1011–1020. [PubMed: 10580986]

Troemel ER, Chou JH, Dwyer ND, Colbert HA, and Bargmann CI (1995). Divergent seven transmembrane receptors are candidate chemosensory receptors in C. elegans. Cell 83, 207–218. [PubMed: 7585938]

Ward JD (2015). Rapid and precise engineering of the Caenorhabditis elegans genome with lethal mutation co-conversion and inactivation of NHEJ repair. Genetics 199, 363–377. [PubMed: 25491644]

Ward S, Thomson N, White JG, and Brenner S (1975). Electron microscopical reconstruction of the anterior sensory anatomy of the nematode Caenorhabditis elegans.?2UU. J. Comp. Neurol 160, 313–337. [PubMed: 1112927]

Waterhouse AM, Procter JB, Martin DMA, Clamp M, and Barton GJ (2009). Jalview Version 2—a multiple sequence alignment editor and analysis workbench. Bioinformatics 25, 1189–1191. [PubMed: 19151095]

Wicks SR, Yeh RT, Gish WR, Waterston RH, and Plasterk RH (2001). Rapid gene mapping in Caenorhabditis elegans using a high density polymorphism map. Nat. Genet 28, 160–164. [PubMed: 11381264]

Zuryn S, Le Gras S, Jamet K, and Jarriault S (2010). A strategy for direct mapping and identification of mutations by whole-genome sequencing. Genetics 186, 427–430. [PubMed: 20610404]

Highlights

- The glial GPCR REMO-1 regulates stress-induced neural plasticity in *C. elegans*

- REMO-1 functions cell-autonomously to regulate glial and neuronal remodeling

- REMO-1-dependent remodeling primes animals to respond to favorable conditions
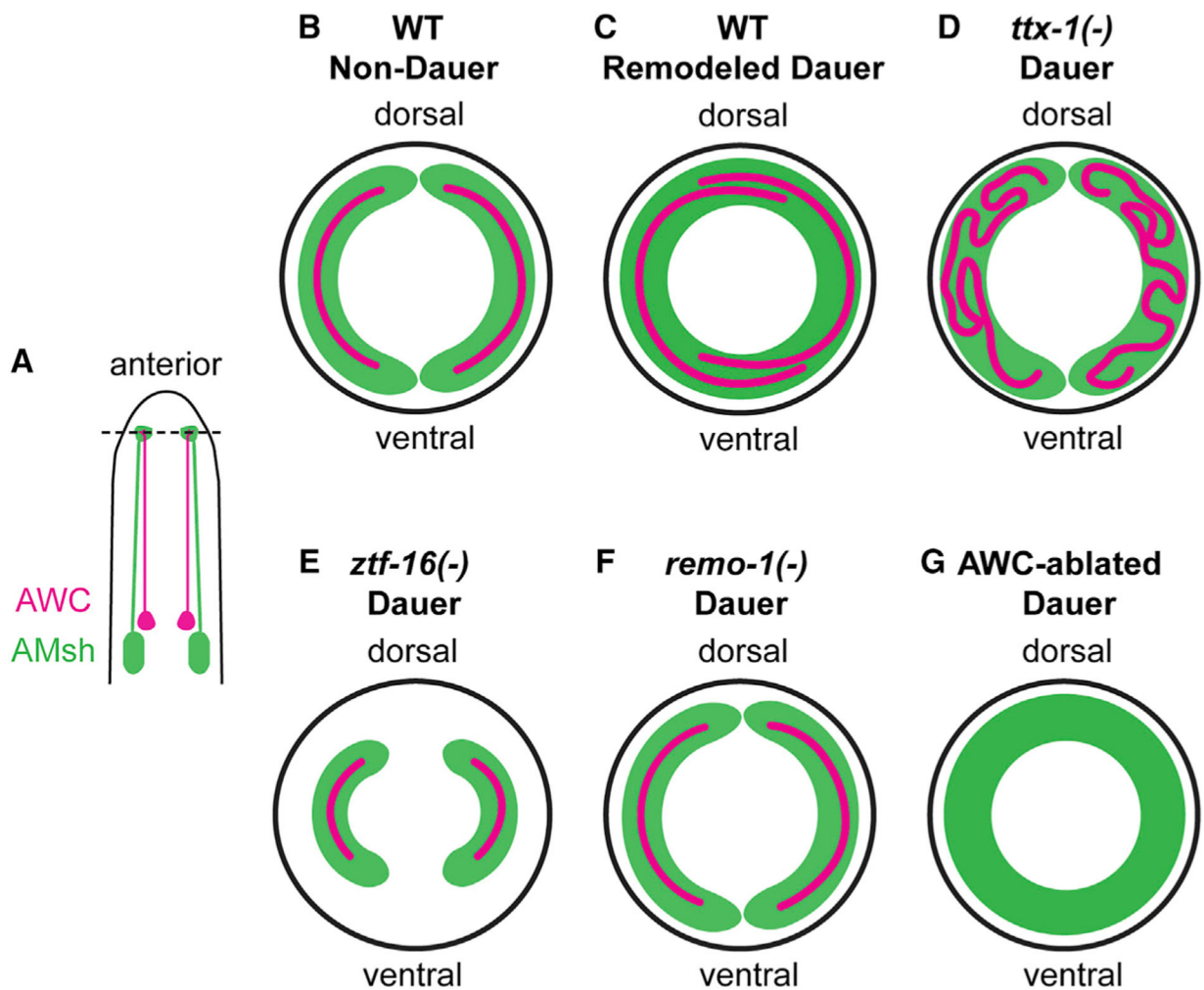
Figure 1. Schematic of Amphid Sensory Organ Remodeling in *C. elegans* Dauer Animals

(A) Schematic of the head of the animal, showing the two bilateral AMsh glia (green) and AWC sensory neurons (red). The horizontal dashed line indicates the position of the transverse sections shown in (B)–(G).

(B–G) Sections through the nose tip showing the relative positions of the AWC neuron receptive ending and the ensheathing AMsh glia in wild-type non-dauer (B), dauer (C), *ttx-1(p767)* (D), *ztf-16(ns171)* (E), *remo-1(ns250, −820, −821)* (F), and AWC-ablated (G) dauer animals. Not to scale. (D) and (E) are based on Procko et al. (2011).
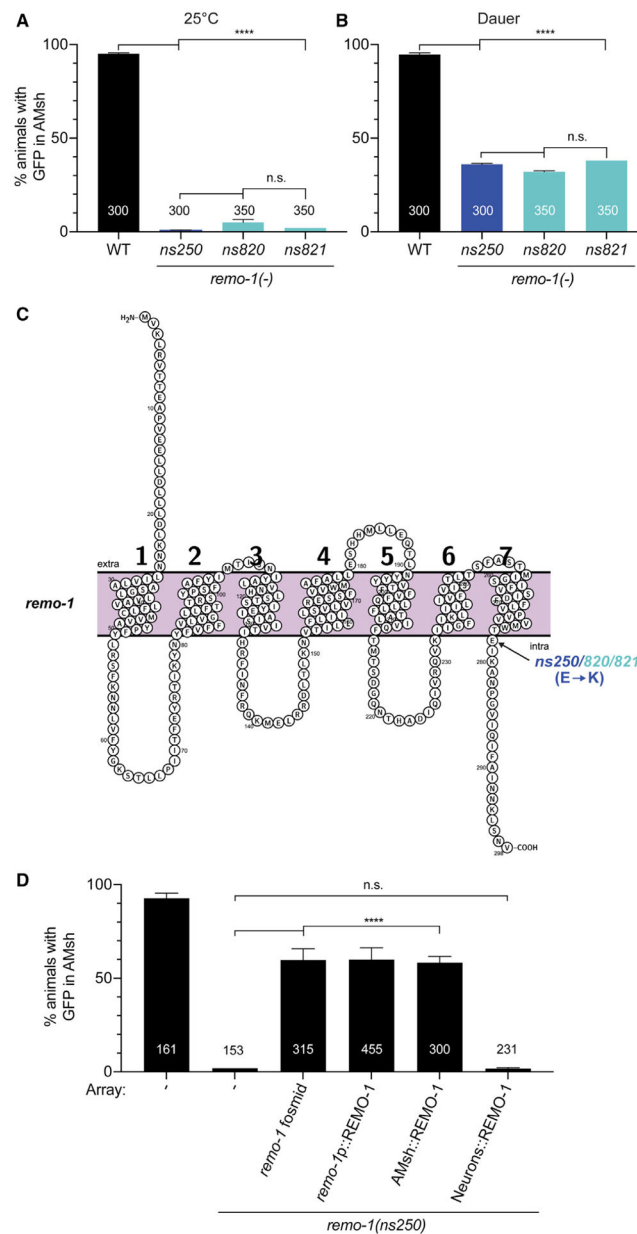
See also Figure S4B.

Figure 2. Glial REMO-1 Regulates Stress-Induced VER-1/RTK Expression

(A and B) *ver-1*p::GFP expression in the AMsh glia in indicated genotypes at 25°C in young adult (A) or in dauer larvae induced by starvation (B). WT, wild-type. The number of animals scored is inside bars. Error bars denote SEM of three independent scoring experiments. n.s., $p > 0.05$; ****$p < 0.0001$.

(C) Diagram of REMO-1 predicted protein structure and mutation sites generated with Protter software. *ns250/820/821*: glutamic acid-to-lysine change at position 278 (E278K) indicated by arrow.

(D) Histogram detail as in (A) and (B). All strains are in a *remo-1(ns250)* mutant background, except for wild-type animals on the left. Rescue experiments conducted with genomic fosmid rescue construct WRM0638cF08, which spans the *remo-1* locus, a smaller

remo-1 genomic fragment, an AMsh glia promoter (*F16F9.3*) driving *remo-1* cDNA, or amphid sensory neuron promoter (*dyf-7*) driving *remo-1* cDNA. All rescue constructs were injected with a co-injection marker (*unc-122*p::RFP). Animals were screened at young adult stage. Three independent lines were observed for each rescue construct.
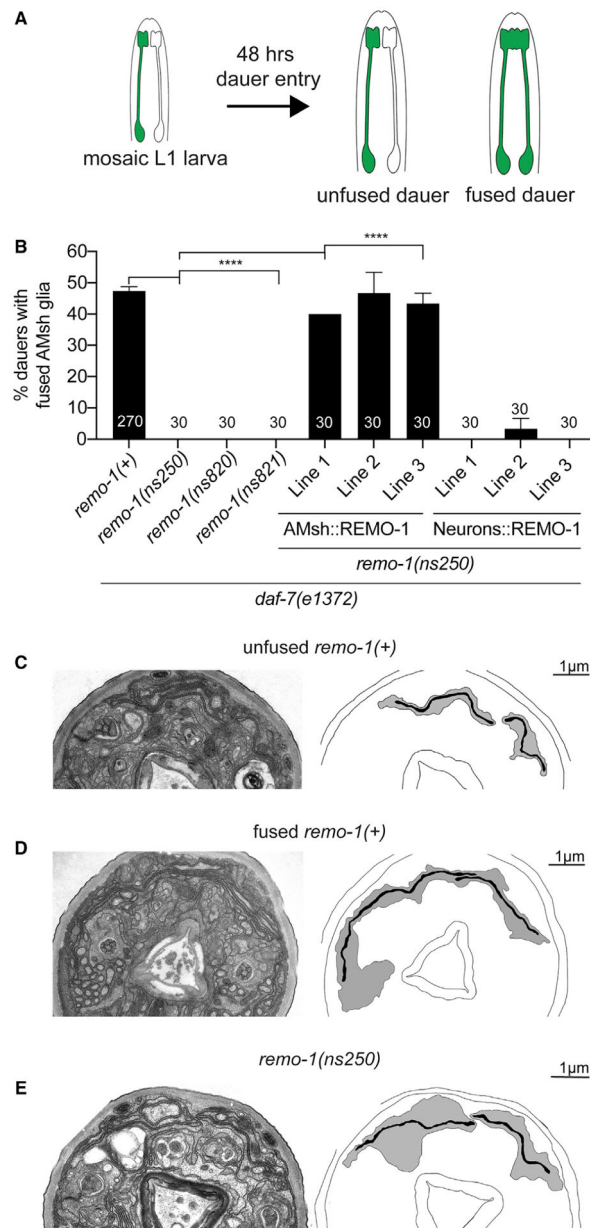
See also Figure S1.

Figure 3. REMO-1 Functions in AMsh Glia to Regulate Dauer-Induced AMsh Glia Remodeling

(A) Cytoplasmic mixing assay. Schematic of the head of the animal, which expresses an AMsh::GFP transgene from an unstable extrachromosomal array (*nsEx1391*). Anterior is up. See STAR Methods. Adapted from Procko et al. (2011).

(B) Percentage of animals with fused AMsh glia as scored by cytoplasmic mixing assay in indicated genotypes. All strains carry the *daf-7(e1372)* mutation to induce dauer when cultivated at 25°C. Cell-specific expression of *remo-1* in AMsh glia (*F16F9.3* promoter) rescues dauer-induced AMsh glia fusion, whereas expression in the amphid neurons (*dyf-7* promoter) does not. Rescue experiments were conducted in *remo-1(ns250)* mutant background, and three independent extrachromosomal arrays were observed per rescue

construct. Number of animals scored is inside bars. Error bars denote SEM of at least three independent scoring experiments. ****p < 0.0001.

(C–E) Representative electron micrographs (EMs) and schematic outlines of amphid sensory organs in dauer animals of given genotypes. Dauer larvae were induced by the *daf-7(e1372)* mutation cultivated at 25°C. Scale bar, 1 μm.
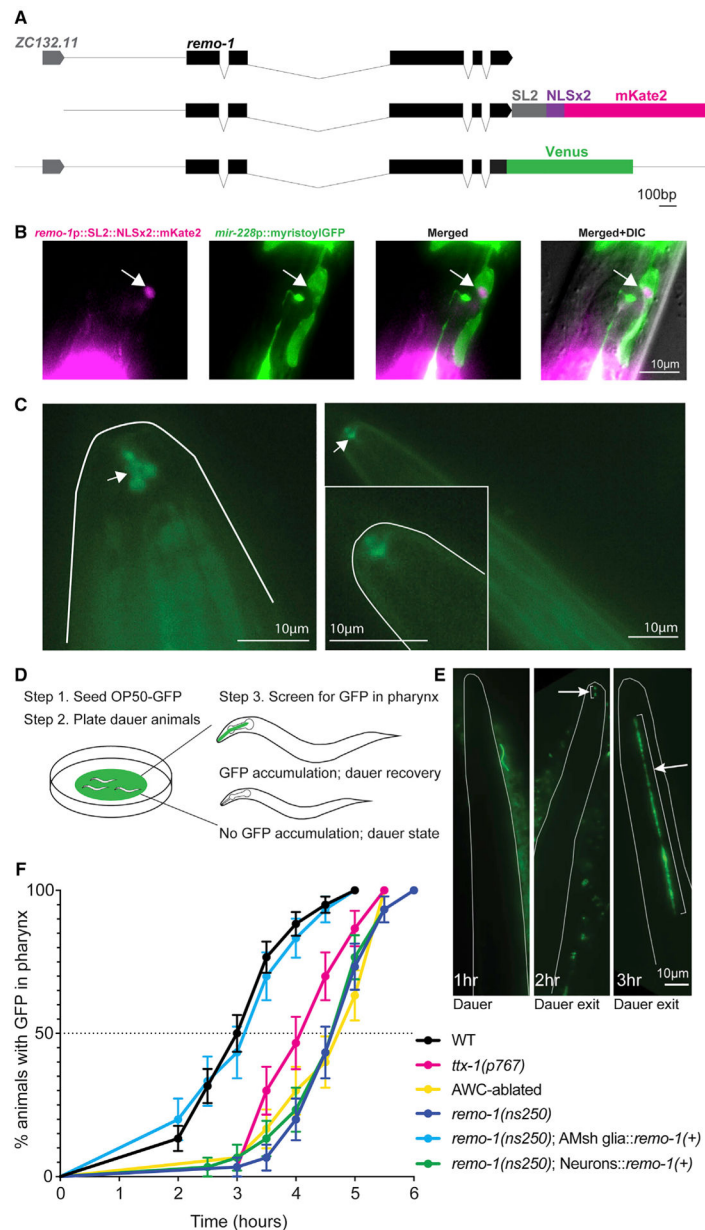
Figure 4. REMO-1 Is Expressed and Localized at the Tip of the AMsh Glia to Regulate Dauer Exit Timeline

(A) Top: schematic of *remo-1* and its upstream gene, *ZC132.11*. Middle: *remo-1* transcriptional reporter. Bottom: *remo-1* translational reporter. Black boxes represent exons, black lines indicate introns, and gray line indicates 5′ intergenic region. Scale bar, 100 bp.

(B) Fluorescence images depicting expression of *remo-1* transcriptional reporter co-expressed with a pan-glial *mir-228*p::myristoylGFP transgene. *remo-1* promoter expression in AMsh glia (left, arrow); *mir-228* pan-glial promoter expression (middle left, AMsh glia arrow); merged (middle right; AMsh glia arrow); merged with DIC (right, AMsh glia arrow).

(C) Fluorescence images depicting subcellular localization of REMO-1 in AMsh glia (arrow) in adult (left) and dauer (right) animals. REMO-1 accumulates at the tip of the amphid region. Adult animals were cultivated at 25°C, and dauer state was induced by

starvation. Magnified inset of the Venus accumulation at the tip of the nose. In (B) and (C), scale bar, 10 μm.

(D) Dauer recovery assay. See STAR Methods.

(E) Fluorescence images showing timeline of GFP-tagged OP50 bacteria accumulation in the pharynges of dauer animals cultivated at 15°C. Images are maximum z stack projections of the entire head volume of the animal. Outline of the animal is marked in gray. Arrow marks the accumulation of GFP-tagged OP50 bacteria in the pharynx. Anterior is up. Time in hours following exposure to GFP-tagged OP50 bacteria. Each image is of a different animal. Scale bar, 10 μm.

(F) The rates of dauer exit measured by the onset of GFP-tagged OP50 bacteria accumulation in the pharynx. Black dotted line indicates the time point at which 50% of the given population recovers pumping. *ttx-1(p767)*, AWC-ablated, and *remo-1(ns250)* mutants show significant dauer exit delay compared with wild-type ($p < 0.0001$). Dauer exit delay in *remo-1(ns250)* is rescued by restoring WT REMO-1 in AMsh glia (*F16F9.3* promoter) but not in amphid sensory neurons (*dyf-7* promoter). Dauer larvae induced by starvation. Error bars denote SEM of at least three independent scoring experiments.

See also Figures S2A, S2B, and S4A.

KEY RESOURCES TABLE

REAGENT or RESOURCE	SOURC...
Bacterial and Virus Strains	
E. coli OP50	Caenor... Center ... cbs.um...
E. coli OP50-GFP	CGC
Experimental Models: Organisms/Strains	
C. elegans: N2	CGC
Oligonucleotides	
REMO-1(E278K) sgRNA: 5′ TCCAGTGGTTGTCATGTGGA 3′	This stu...
REMO-1(deletion/premature stop) sgRNA #1: 5′ GCGTTTGTTCAAGCAACATG 3′	This stu...
REMO-1(deletion/premature stop) sgRNA #2: 5′ AATTCTGAGTGTTTTGGTGA 3′	This stu...
REMO-1::VENUS sgRNA: 5′ ACGGAAATCAAAGCGAACCC 3′	This stu...
Single stranded repair oligo REMO-1(E278K): 5′ TATTTGTGAGTATCGATTTCTTCCTTGTTCCAGTGGTTGTCATGTGGACGaAAATCAAAGCGAACCCGGGTGTTATTCAGATTTTTGCAATTAACAACAAA 3′	This stu...
REMO-1::VENUS homologous repair template (detail in methods)	This stu...
Recombinant DNA	
pDD162	(Dickin...
pIHL164: *remo-1*[E278K] CRISPR targeting vector #1, pDD162 backbone	This stu...
pIHL212: *remo-1*[deletion/premature stop] CRISPR targeting vector #1, pDD162 backbone	This stu...
pIHL213: *remo-1*[deletion/premature stop] CRISPR targeting vector #2, pDD162 backbone	This stu...
pIHL217: *remo-1*[Venus] CRISPR targeting vector, pDD162 backbone	This stu...
Fosmids WRM0638cF08	Source ... www.s...
*nsIs22: ver-1*p::GFP	(Procko...
nsEx6181, −82, −83: remo-1 fosmid (WRM0638cF08) (20 ng/µl) + *unc-122*p::RFP (20 ng/µl) + pBluescript (60 ng/µl)	This stu...
nsEx6184, −85, −86: remo-1 gDNA (50 ng/µl) + *unc-122*p::RFP (20 ng/µl) + pBluescript (30 ng/µl)	This stu...
*nsEx6048, 6173, 6174: F16F9.3*p::remo-1 cDNA (40 ng/µl) + *unc-122*p::GFP (20 ng/µl) + pBluescript (40 ng/µl)	This stu...
nsEx6045, −46, −47: *dyf-7*p::remo-1 cDNA (40 ng/µl) + *unc-122*p::GFP (20 ng/µl) + pBluescript (40 ng/µl)	This stu...
*nsIs391: mir-228*p::myr-GFP + *lin-15*(+)	This stu...
nsEx6249: pIHL28[*remo-1*p::SL2-NLSx2-mKate2] (90 ng/µl) + *unc-122*p::RFP (10 ng/µl)	This stu...
*nsEx1391: F16F9.3*p::GFP + pRF4[*rol-6*(*su1006*)]	(Procko...
*nsIs855: (F28A12.3*p::myr-GFP)	This stu...
*nsEx1942: ttx-1*p::GFP + pRF4[*rol-6*(*su1006*)]	(Procko...
*nsEx3001: R08E3.4*p::GFP + pRF4[*rol-6*(*su1006*)]	(Procko...
*nsEx2727: F16F9.3*p::*aff*-1 cDNA-GFP + pRF4[*rol-6*(*su1006*)]	(Procko...
*nsEx6027: unc-122*p::RFP (20 ng/µl) + pBluescript (80 ng/µl)	This stu...
nsEx6125, −26, −27: pIL20 [*F16F9.3*p::REMO-1 E278K] (10 ng/µl) + *unc-122*p::GFP (20 ng/µl) + pBluescript (70 ng/µl)	
*oyIs85: ceh-36*p::TU#813 + *ceh-36*p::TU#814 + *srtx-1*p::GFP + *unc-122*p::DsRed]. TU#813 and TU#814 are split caspase vectors (Chalfie Lab) subcloned downstream of the *ceh-36* promoter.	CGC; (...
Software and Algorithms	
Prism 8	GraphP...

REAGENT or RESOURCE	SOURC
ImageJ	(Schnei
Protter	(Omasi
Jalview	(Waterh